Id.: EN-25

NEUTRONIC ANALYSIS OF THE NC-9000 SUBCRITICAL NUCLEAR REACTOR

Jefferson Q. C. Duarte[1], Thalles O. Campagnani[1], Carlos E. Velasquez[1]

[1] UFMG, Av. Pres. Antônio Carlos, 6627, Escola de Engenharia, Bloco 4, DEN
Pampulha, Belo Horizonte - MG, 31270-901
jefferson9@ufmg.br

Keywords: Neutronic Analysis, OpenMC, Subcritical Nuclear Reactor, NC-9000

ABSTRACT

This paper presents a neutronic analysis to assess the reactor characteristics of the NC-9000 model, a tank-type subcritical reactor from the UFMG (Universidade Federal de Minas Gerais), manufactured by Nuclear Chicago Corporation. A model was developed and compared with reference data, including a comparison with the manufacturer's report and a study using the same model, differing only in fuel density. To achieve this purpose, the effective multiplication factor, subcritical multiplication factor, and neutron amplification factor were calculated. Additionally, neutron flux mapping was performed across the reactor, considering thermal and fast energy groups, while the irradiation region positions were assessed for potential educational experiments and research activities within the DEN (Departamento de Engenharia Nuclear), in case of its future installation in the department. Simulation results reveal that k_{eff} was determined to be 0.841897, closely aligning with the manufacturer's value of 0.842. Additionally, a simulation of NC-9000 done by Vega-Carrillo, Garcia-Reyna, Marquez-Mata, *et al.* [1] shows good agreement with this work, differing only by 1.46%, likely due to variations in fuel density. However, results reported by Motta [2], which are heavily affected by a large margin of error, differs significantly from this work. Since the source is positioned within the nuclear system, k_s exceeds k_{eff} and shows a conservative estimation. The neutron amplification factor (M), directly dependent of k_s, shows a net neutron increase by a factor of 11 in relation to the total emitted by the source. Thermal neutron flux reached a maximum of 2.4×10^4neutrons $\cdot\, \mathrm{cm}^{-2} \cdot \mathrm{s}^{-1}$, while fast neutrons peaked at 1.6×10^5neutrons $\cdot\, \mathrm{cm}^{-2} \cdot \mathrm{s}^{-1}$. In regard to irradiation positions, inside the annular fuel the ideal irradiation zone was a cylinder with a diameter of $1.27\,\mathrm{cm}$ and a height of $22.74\,\mathrm{cm}$, with thermal and fast fluxes averaging 1.48×10^4neutrons $\cdot\, \mathrm{cm}^{-2} \cdot \mathrm{s}^{-1}$ and 5.70×10^4neutrons $\cdot\, \mathrm{cm}^{-2} \cdot \mathrm{s}^{-1}$, respectively. The optimal region for irradiation above the source was identified as a cylinder measuring $3.32\,\mathrm{cm}$ in diameter and $4.60\,\mathrm{cm}$ in height, where the thermal flux achieved 2.48×10^4neutrons $\cdot\, \mathrm{cm}^{-2} \cdot \mathrm{s}^{-1}$ and the fast flux reached 4.25×10^4neutrons $\cdot\, \mathrm{cm}^{-2} \cdot \mathrm{s}^{-1}$. Simulation results were generated using the OpenMC Monte Carlo code, employing the nuclear data library *ENDF/B-VIII.0*. Data analysis and various types of plots were conducted using Matplotlib.

1. INTRODUCTION

In decade of 1960's, ITA (Instituto Tecnológico de Aeronáutica) inaugurated a subcritical nuclear reactor of model NC-9000 (Nuclear Chicago 9000) manufactured by Nuclear Chicago Corporation, from U.S.A. Later, in the 1990's it was donated to the Universidade Federal de Minas Gerais - (UFMG). The parts of the reactor, shown in Fig. 1, comprise a tank-type subcritical reactor moderated and reflected by light water, fueled with natural uranium.

The reactor core has a single fuel element composed of 282 fuel rods arranged in a hexagonal matrix, with an additional 30 positions available for rods of any material in the peripheral regions of the

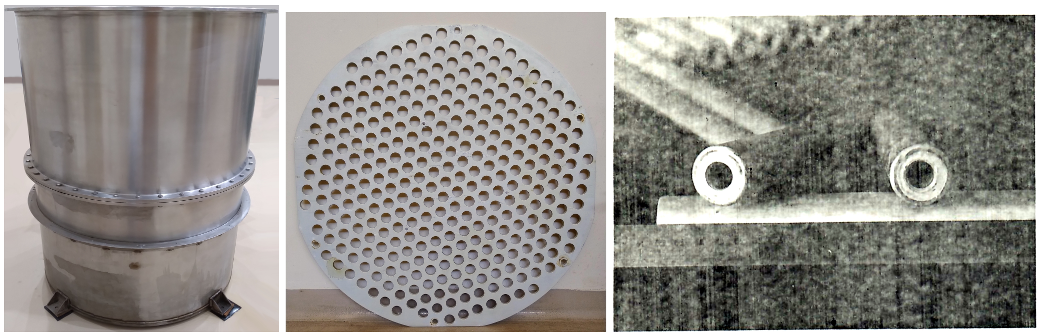

(a) Reactor tank (SS304) (b) Hexagonal Grid Support (c) Small fuel bars [2]

Figure 1. Photos of reactor components.

reactor core, allowing for the rearrangement of rods as needed. The central tube is filled with water and contain space for the neutron source allocation and for sample irradiation.
The remaining rods are filled with air, each one houses five cylindrical annular bars of compacted natural uranium, coated with aluminium, arranged one above the other.
The model NC-9000 is designed with nuclear and radiological safety in mind, allowing users, including students and faculty, to perform tasks such as inserting or removing detectors, irradiating samples, handling fuel rods, and conducting measurements [3].
Currently, the fuel rods are under a safeguard system of Comissão Nacional de Energia Nuclear - (CNEN), pending commissioning of nuclear installation at DEN/UFMG (Departamento de Engenharia Nuclear da UFMG).
A master's dissertation from Motta [2] (ITA, 1970) analyzed the characteristics of this reactor, where it was found that some data provided by the manufacturer were incorrect. For example, the manufacturer provided the pitch distance (distance between the centers of two closest bars) as $1.75\,\mathrm{in}$, while measuring the hexagonal grid (Fig. 1b) it was found that it is actually $2\,\mathrm{in}$. Since the geometry has changed, it would inferred that there are differences in the effective multiplication factor, between the real value and the one provided by the manufacturer.
Given the discrepancies in the information provided by the manufacturer, and considering that now, there is availability of computational tools for the neutronic analysis, such as Monte Carlo simulation, it is important for DEN to conduct a neutronic study to assess the reactor's characteristics in case of future installation. For this purpose, is calculated the effective multiplication factor, source multiplication factor and neutron amplification factor. After that, the neutron flux is mapped throughout the reactor, considering two energy groups: thermal and fast. Then, the neutron flux is assessed in the irradiation regions positions, considering these thermal and fast energy groups and the neutron flux spectrum in the irradiated regions.

2. METHODOLOGY

To simulate NC-9000, it is essential that the geometry model and material compositions are aligned with the reference data. Simulation settings should be comprehensively detailed, including the source of input data and the uncertainty margins associated with the results.

2.1. Geometry and Materials

The OpenMC model follows the dissertation by Motta [2] with identical parameters. Complementary data, including stainless steel composition and nuclide information, are drawn from KAERI [4] and Huang, Zhang, Dai, *et al.* [5]. Since, the reference Motta [2] lacks of detail data about the neutron source. Therefore, a closely matching source from the same reactor model (NC-9000) is utilized, described in Section 2.2.
The fuel consists of a annular bar of compacted natural uranium, encased in a $1\,\mathrm{mm}$ aluminium layer on sides and $5\,\mathrm{mm}$ on top and bottom. Each fuel rod is composed of five small bars, totaling 282 fuel rods. These bars weight about $1867\,\mathrm{g}$ each, representing a total of $2630\,\mathrm{kg}$ of natural compacted uranium. To calculate this mass, Motta [2] determined the density using gamma radiography, revealing that the manufacturer's reported density of $18.7\,\mathrm{g\,cm^{-3}}$ was higher, while the measured value was $18.0\,\mathrm{g\,cm^{-3}}$. The fuel has an external diameter of $3.07\,\mathrm{cm}$, an internal diameter of $1.27\,\mathrm{cm}$, and a length of $21.45\,\mathrm{cm}$, as depicted in Fig. 2b.
Light water is used as moderator, coolant, and reflector, requiring de-ionization resin treatment to remove dissolved ions. Two types of resins are employed: cationic resins to remove cations and anionic resins to remove anions. The water level is maintained at $135\,\mathrm{cm}$ to ensure is above the fuel. As shown in Fig. 2, there is no reflector material at the top of the reactor; however, there is $16.5\,\mathrm{cm}$ of water at the bottom and $20\,\mathrm{cm}$ at the sides.

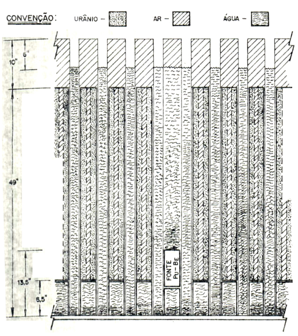

(a) Manual scheme of core.

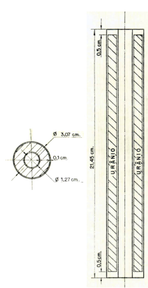

(b) Diagram of gamma imaging for one small fuel bar.

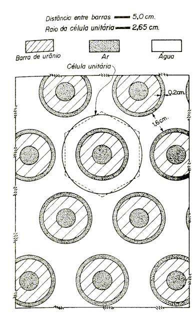

(c) Unit cell diagram.

Figure 2. Geometric configuration acording Motta [2]

Fuel rods are arranged in a hexagonal grid with a pitch distance of $5.08\,\mathrm{cm}$, and the entire core is housed in a cylindrical vessel with a height of $150\,\mathrm{cm}$ and a diameter of $122\,\mathrm{cm}$ made of stainless steel and has a thickness of $1.2\,\mathrm{cm}$. Furthermore, the upper hexagonal grid is positioned $28.4\,\mathrm{cm}$ above the vessel's bottom, while the lower grid is fixed at the bottom with a space of $2.54\,\mathrm{cm}$.
This reactor model was developed in *OpenMC 0.15.0* [6], as shown in Fig. 3.
It is worth to note that the source of neutrons is positioned at the center of the fuel, and the nuclear data library for photons and neutrons used in this work is *ENDF/B-VIII.0*. As this is a zero-power reactor designed for research purposes, the fuel temperature and all other materials are set to ambient temperature, specifically $294\,\mathrm{K}$.

2.2. Neutron Source

Three $^{239}\mathrm{PuBe}$ neutron source cylinders located in the center of the core were used in the ITA's reactor, as described by Motta [2]. These sources were provided by the Nuclear Material and

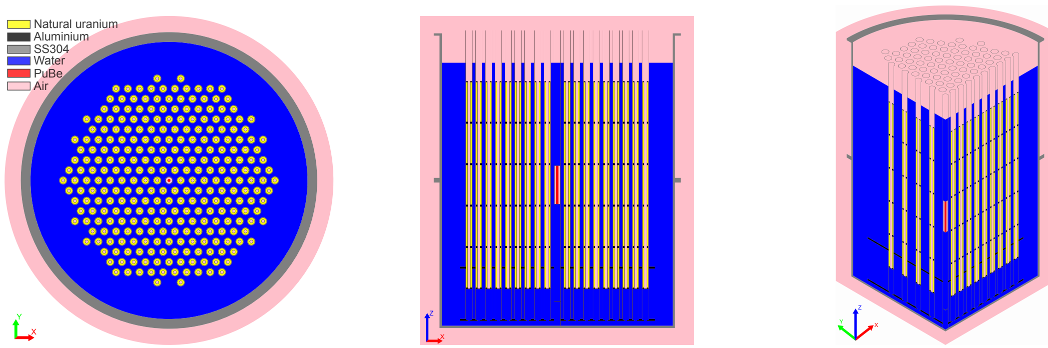

(a) Top view, sectioned along the central axis.

(b) Side view, sectioned along the middle plane.

(c) 3D view, sectioned along the middle plane and top of reactor tank.

Figure 3. Geometric configuration modelled in *OpenMC*.

Equipment Corporation in Pennsylvania. They contain $80\,\mathrm{g}$ of plutonium and have a total activity of $0.185\,\mathrm{TBq}$. The neutron sources are in a cylindrical stainless steel containers, which are secured inside an aluminum tube with a diameter of $3\,\mathrm{cm}$ and a length of $20\,\mathrm{cm}$. The neutron yields are 1.87×10^6 , 3.53×10^6 , and 3.86×10^6 neutrons/s, totaling a source strenght of 9.26×10^6 neutrons/s. Thus, this work uses a very similar $^{239}\mathrm{PuBe}$ source described by Vega-Carrillo, Hernández-Dávila, Rivera, *et al.* [7].
This source contains approximately $80\,\mathrm{g}$ of plutonium and $40\,\mathrm{g}$ of beryllium, with a $^{239}\mathrm{Pu}$ isotopic fraction of 0.9301. Considering isotopic fractions of 0.0676 and 0.0023 for $^{240}\mathrm{Pu}$ and $^{241}\mathrm{Pu}$, respectively, the source density is approximately $4.6781\,\mathrm{g\,cm^{-3}}$. Manufactured by Monsanto Research Corporation on June 22, 1967, the source initially had a nominal $^{239}\mathrm{Pu}$ activity of $0.185\,\mathrm{TBq}$ and a neutron yield of 9.04×10^6 neutrons/s. Over time, the reduction in neutron yield due to $^{239}\mathrm{Pu}$ decay has been offset by the increased yield from rising $^{241}\mathrm{Pu}$ impurities. As a result, after 44 years, the source has a neutron yield of 1.01×10^7 neutrons/s. The emission spectrum of the source is discretized into nine distinct energy levels: 3.7×10^4, 7.8×10^4, 1.7×10^5, 3.1×10^5, 7.0×10^5, 1.0×10^6, 2.9×10^6, 5.6×10^6 and 1×10^7 eV, with corresponding emission probabilities of 0.115, 0.289, 0.641, 1.48, 7.05, 10.9, 14.8, 26.9 and $37.8\,\%$, respectively.

2.3. Simulation Settings

To simulate with accuracy, an *OpenMC* cluster compiled with *OpenMP* and *OpenMPI* was developed. It is composed by 6 processors, totaling 80 cores and 160 threads, distributed across 4 servers. With this computational power, it was possible to perform in a timely manner fixed source simulations with 100 cycles and 1×10^7 particles, and eigenvalue simulations with 1000 active cycles, 200 skipping cycles and also 1×10^7 particles. This configuration was enough to achieve convergence of the k-eigenvalue and neutron source distribution.

2.4. Analysis and Uncertainty Quantification

The simulation settings are sufficient to keep the relative uncertainties of the tallies below 5%, including error propagations. The remaining uncertainties are presented as standard deviation.

2.4.1. Neutronic Paramethers

It is important to determine some key neutronic parameters for subcriticals systems: multiplication factor (k_{eff}), subcritical multiplication factor (k_s), neutron amplification factor (M) and the importance of external neutron source (ϕ^*). The parameter k_s represents the fraction of neutrons generated by fission relative to the total neutron population. So, it depends of both: the subcritical reactor system and the external source. And its directly related to M, which is the ratio of total source to fixed source. These parameters are calculated using numerical methods, as shown in Eq. (2.1) [8].

$$k_s = \frac{F}{F+S}; \qquad M = \frac{1}{1-k_s}; \qquad \phi^* = \frac{1-\frac{1}{k_{eff}}}{1-\frac{1}{k_s}}, \tag{2.1}$$

where F represents the neutrons generated by fission, S represents the neutrons originating from the source.

According to the results of Shi, Zhu, and Tao [8] “the parameter measured by the source multiplication method actually is a subcritical effective neutron multiplication factor k_s with an external neutron source, not the effective neutron multiplication factor k_{eff}”.

2.4.2. Spacial and spectrum flux distribution

All the spatial fluxes were divided into 2 energy ranges, namely:

- Thermal range: from 1×10^{-5} eV to 1.0 eV;
- Fast range: from 1.0 eV to 1.1×10^{7} eV.

Considering the cylindrical geometry of the reactor core, radial and axial meshes were created for neutron counting. For the radial flux, a rectilinear mesh divided into 284^2 parts in 2 directions ($\vec{X}$ and $\vec{Y}$) was used to allow a 2D visualization of flux intensity, in addition to a narrow rectangular mesh divided into 1000 parts in 1 direction ($\vec{X}$) for a more detailed visualization of flux variation along the different parts of the reactor. Fig. 4a and Fig. 4b show the position and geometry of rectilinear meshes on cross-sectional views of reactor.

For the axial flux, two axial meshes were created in two different positions: a cylindrical mesh divided into 1000 parts on $\vec{Z}$ direction inside the central rod, and another mesh inside one of six fuel rod closest to central rod, divided the same amount of parts and same direction. The axial meshes were positioned in these locations also considering the possibility of their use for sample irradiation, as they are theoretically locations with the highest flux intensity as they are closer to the center of the reactor and the neutron source at the same time. This statement is verified by tally results corresponding to the previously described regions. Fig. 4a and Fig. 4b also show the position and geometry of axial meshes on cross-sectional views of reactor.

Considering that the highest flux positions within central and fuel rods are closest to the center and source, two meshes were created in available irradiation regions with high flux to investigate the spectrum a sample would be subjected to:

(1) Positioned above source, inside central tube, arbitrated $1\,\mathrm{cm}$ hight; and
(2) Positioned inside the fuel, internal diameter of the fuel, same size and $\vec{Z}$ position as the source.

Fig. 4c show the position and geometry of axial meshes on cross-sectional views of reactor. The spectrum are divided on 150 energy intervals, from 1×10^{-5} to 1×10^{7} eV.

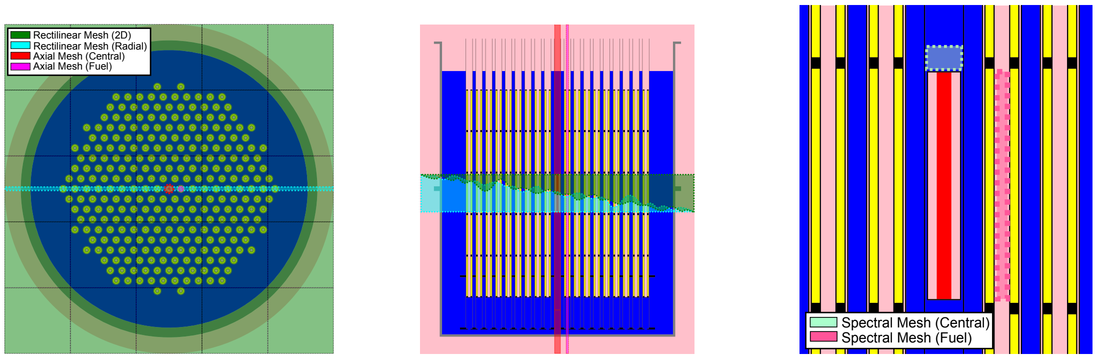

(a) Top view of spacial meshes. (b) Side view of spacial meshes*. (c) Side view of spectral meshes.

Figure 4. Geometric configuration of meshes in *OpenMC*.
*Blue and green regions overlap because they have same size on $\vec{X}$ and $\vec{Z}$ directions.

3. RESULTS

3.1. Neutronic Behavior and Multiplication Factors Analysis

Tab. 1 compares the value of k_{eff} obtained from simulation (Simu.) performed in this work with values of reference data: Provided by the Manufacturer (Manu.) according to Motta [2]; the Experiments (Exp.) performed by Motta [2]; the Calculations (Calc.) performed by Motta [2]; and the Simulation performed by Vega-Carrillo, Garcia-Reyna, Marquez-Mata, *et al.* [1].

Table 1. Comparison of k_{eff} from simulation performed in this work with other sources. Difference is from k_{eff} simulated in this work to other sources (PCM) and uncertainty is in standard deviation.

Source	Simu.	Manu. [2]	Exp. [2]	Calc. [2]	Simu. [1]
k_{eff} **mean value**	0.841 897	0.842	0.96	0.91	0.8296
Uncertainty	9×10^{-6}	-	-	7×10^{-2}	6×10^{-4}
Difference (PCM)	-	10	11 810	6810	1230

Simulated k_{eff} closely aligns with manufacturer data, differing by only 10 PCM. The calculation from Motta [2] shows a larger difference of 6810 PCM compared to this work, with a significant margin of error, potentially reaching a lower value of 0.84. Experimentally, this estimate goes even higher reaching a difference of 11 810 PCM. The author do not present the uncertainty of the result and concluded that the experimental results are difficult to interpret.
A similar simulation done by Vega-Carrillo, Garcia-Reyna, Marquez-Mata, *et al.* [1], shows a slightly lower k_{eff} than the obtained in this work, showing a difference of 1230 PCM. It was also based on 282 fuel rods, but presents a lower density of compacted natural uranium, reported as $14.01\,\mathrm{g\,cm^{-3}}$, while the fuel simulated in this work has a density of $18\,\mathrm{g\,cm^{-3}}$, which justifies the difference in the k_{eff} value obtained in both simulations.
As depicted in Tab. 2, the mean value of k_s is higher than k_{eff}, indicating a conservative estimate for cases where the external source is inside the system. The significant contribution of the source

to the neutron population is indicated from $\phi^* > 1$, implying that one external source neutron corresponds to 1.87 fission neutrons [8]. In a steady-state subcritical system approaching criticality, the neutron flux distribution becomes similar to that of a critical system with external sources included. Consequently, the value of k_s tends to approximate of k_{eff}, which is not the case here. Finally, the mean value of M indicates a net neutron increase of approximately $11\times$ the total neutrons emitted by the source.

Table 2. Subcritical multiplication factor of NC-9000 and related parameters.

Parameters	k_s	ϕ^*	M
Mean value	0.908850	1.872485	10.970965
Uncertainty	1.58×10^{-4}	2.83×10^{-5}	1.90×10^{-2}

The neutron flux distribution, shown in Figs. 5a and 5c, is divided into thermal and fast energy groups. In the thermal group, a cavity appears in the center of the graph due to the presence of the source. Beyond the surface of the source, neutrons begin to moderate, reaching a peak thermal flux of approximately 2.4×10^4 neutrons $\cdot\, \mathrm{cm}^{-2} \cdot \mathrm{s}^{-1}$. The graph also illustrates the reflection effect on neutrons as they attempt to pass through the $20\,\mathrm{cm}$ water column along the reactor's sides. In the fast group, as expected, the peak occurs at the center, with a flux of around 1.6×10^5 neutrons $\cdot\, \mathrm{cm}^{-2} \cdot \mathrm{s}^{-1}$, rapidly decreasing as the distance from the center increases. Neutron interactions across the reactor geometry are clearly visible in Fig. 5b. This radial flux profile allows us to make four observations: (1) the various peaks in thermal neutrons correspond to water-filled regions between the fuel rods, while the small peaks in fast neutrons represent areas containing fuel; (2) the double valleys in thermal flux are caused by capture reactions in the annular fuel; (3) the maximum flux in the lateral reflector zone is 1.23×10^3 neutrons $\cdot\, \mathrm{cm}^{-2} \cdot \mathrm{s}^{-1}$; and finally, (4) the peak thermal flux directly correlates with previous data, reaching 2.38×10^4 neutrons $\cdot\, \mathrm{cm}^{-2} \cdot \mathrm{s}^{-1}$.

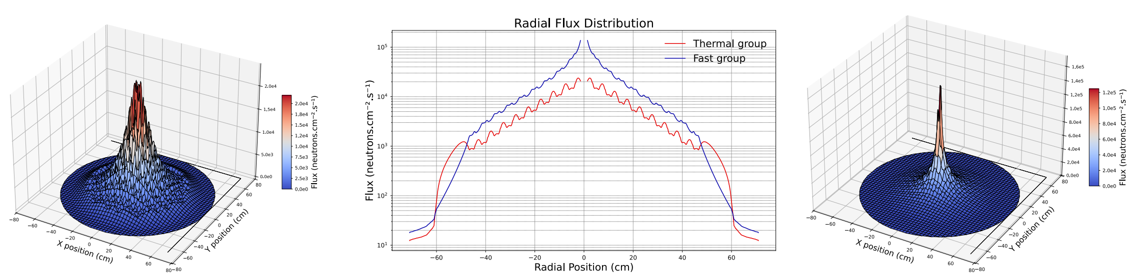

(a) Neutron flux distribution for the thermal energy group. (b) Radial neutron flux distribution surrounding the centralized source. (c) Neutron flux distribution for the fast energy group.

Figure 5. Spatial spectra of flux for two energy groups.

3.2. Irradiation Positions Analysis

As described previously, this section focuses on studying the neutron flux in two potential regions of interest for irradiation. On the one hand, Fig. 7 shows the energy spectra of the flux in both regions. For high-energy neutrons, above $0.1 \times 10^6\,\mathrm{eV}$, both regions exhibit similar behavior, differing only in the flux intensity. These high-energy neutron peaks reflect the discretization of the

PuBe neutron source's emission spectrum, where larger peaks correspond to higher probabilities of neutron emission. Above the source, for neutrons below $4 \times 10^2\,\mathrm{eV}$, the energy group changes rapidly, while the flux remains almost constant. A similar pattern is observed for neutrons within the annular fuel. However, in the resonance range from 5.0 to $1.39 \times 10^2\,\mathrm{eV}$, neutron flux decreases by up to approximately 73%. In the thermal range, flux inside the annular fuel is lower due to radiative capture in uranium isotopes, with the peak being about 39% lower compared to above the source. To better evaluate neutron flux and the available space for efficient sample irradiation, a precise axial spatial spectrum was created, as shown in Fig. 6.

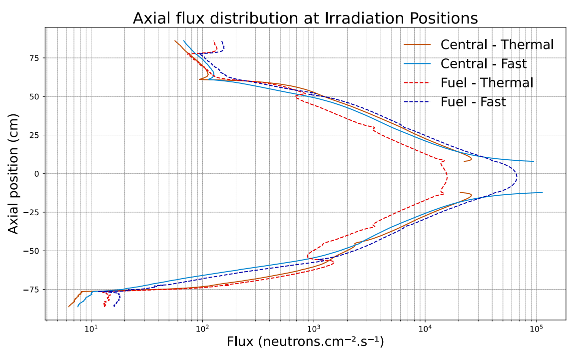

Figure 6. Axially divided spatial spectra of flux for two energy groups.

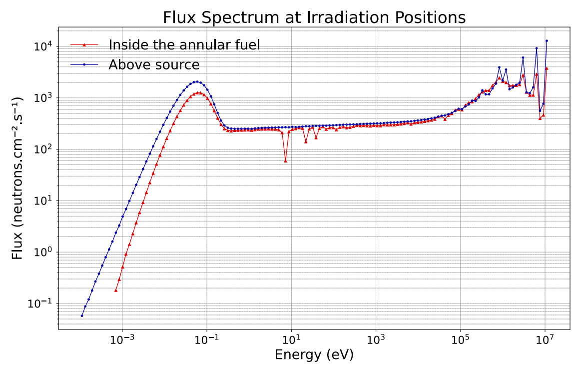

Figure 7. Energy spectra of flux in two regions: (1) inside the annular fuel closest to the center, and (2) above the source.

Inside annular fuel, the optimal region for irradiation applications is a cylinder with a diameter of $1.27\,\mathrm{cm}$ and a height of $22.74\,\mathrm{cm}$. This area averages thermal and fast flux at 1.48×10^4 neutrons $\cdot\,\mathrm{cm}^{-2} \cdot \mathrm{s}^{-1}$ and 5.70×10^4 neutrons $\cdot\,\mathrm{cm}^{-2} \cdot \mathrm{s}^{-1}$, respectively. Above the source, a cylinder with a diameter of $3.32\,\mathrm{cm}$ and a height of $4.60\,\mathrm{cm}$ is the most suitable for such applications. Here, the average neutron flux for thermal neutrons is around 2.48×10^4 neutrons $\cdot\,\mathrm{cm}^{-2} \cdot \mathrm{s}^{-1}$, while for fast neutrons it reaches 4.25×10^4 neutrons $\cdot\,\mathrm{cm}^{-2} \cdot \mathrm{s}^{-1}$.

4. CONCLUSION

This work conducted a neutronic analysis of the subcritical NC-9000, providing data on multiplication factors, flux distributions throughout the reactor and average fluxes at optimized irradiation positions.
Although Monte Carlo simulations require significant computational power, the simulation settings were adequate to maintain the relative error below $5\,\%$ for all tallies and a multiplication factor with a deviation of 9×10^{-6}. The absence of information regarding the original source used by ITA emphasizes the necessity of employing a very similar PuBe neutron source. To address this need, the reference Vega-Carrillo, Hernández-Dávila, Rivera, *et al.* [7], provides comprehensive source data while simulating the same reactor model.
In the first part of results, k_{eff} was determined to be 0.841897, closely aligning with the manufacturer's value of 0.842. This result differs significantly from the data reported by Motta [2], which are heavily affected by a large margin of error. However, this work shows good agreement with the simulation done by Vega-Carrillo, Garcia-Reyna, Marquez-Mata, *et al.* [1], differing only by

1.46%, likely due to variations in fuel density. Since the PuBe source is positioned within the nuclear system, the value of k_s exceeds k_{eff}, leading to a $\phi^* > 1$ and indicating a effective usage of the external neutron source. Taking this into account, ϕ^* equal 1.87 means that one neutron from source corresponds to 1.87 fission neutrons. Additionally, the neutron amplification factor (M) shows a net neutron increase by a factor of 11 in relation to the total emitted by the source. Thermal neutron flux reached a maximum of 2.4×10^4neutrons $\cdot \mathrm{cm}^{-2} \cdot \mathrm{s}^{-1}$, while fast neutrons peaked at 1.6×10^5neutrons $\cdot \mathrm{cm}^{-2} \cdot \mathrm{s}^{-1}$. Neutron moderation, capture in the annular fuel, and reflection from the lateral water layer were key factors affecting the flux distribution.
Second part is focused on studying the neutron flux in two regions of interest for irradiation. The energy spectrum analysis revealed that in resonance range between 5.0 and $1.39 \times 10^2\,\mathrm{eV}$, a significant flux reduction of up to 73% was observed. Thermal neutron flux within the annular fuel was also reduced by approximately 39% due to radiative capture. Inside the annular fuel, the ideal irradiation zone was a cylinder with a diameter of $1.27\,\mathrm{cm}$ and a height of $22.74\,\mathrm{cm}$, with thermal and fast fluxes averaging 1.48×10^4neutrons $\cdot \mathrm{cm}^{-2} \cdot \mathrm{s}^{-1}$ and 5.70×10^4neutrons $\cdot \mathrm{cm}^{-2} \cdot \mathrm{s}^{-1}$, respectively. Above the source, the most suitable region for irradiation was determined to be a cylinder with a diameter of $3.32\,\mathrm{cm}$ and a height of $4.60\,\mathrm{cm}$, where thermal flux reached 2.48×10^4neutrons $\cdot \mathrm{cm}^{-2} \cdot \mathrm{s}^{-1}$ and fast flux 4.25×10^4neutrons $\cdot \mathrm{cm}^{-2} \cdot \mathrm{s}^{-1}$.

ACKNOWLEDGEMENTS

The authors would like to thank funding agency CAPES for the support provided to this work and CDTN/CNEN for providing information and facilitating visits to the disassembled parts of the subcritical reactor.

References

[1] H. R. Vega-Carrillo, M. G. Garcia-Reyna, C. A. Marquez-Mata, J. Vazquez-Bañuelos, G. E. Campillo-Rivera, and S. V. Bedenko, "Effect of changing the neutron moderator in a thermal subcritical nuclear reactor", *Applied Radiation and Isotopes*, vol. 188, p. 110 395, 2022.
[2] F. S. Motta, "Características do reator sub-crítico NC-9000", Master's thesis, Instituto Tecnológico de Aeronáutica - ITA, São José dos Campos, Brasil, 1970.
[3] H. R. Vega-Carrillo, A. L. Aguilar-Dominguez, S. V. Bedenko, and G. F. García-Fernandez, "Computational spectrometry and dosimetry, of neutrons and γ rays, outside a subcritical nuclear reactor with water and polyethylene moderators", *Radiation Physics and Chemistry*, vol. 204, p. 110 719, 2023.
[4] KAERI. "Kaeri nuclear data center - tabelas de núclidos". Accessed: September 5, 2024. (2024), [Online]. Available: `https://atom.kaeri.re.kr/`.
[5] W. Huang, Y. Zhang, W. Dai, and R. Long, "Mechanical properties of 304 austenite stainless steel manufactured by laser metal deposition", *Materials Science and Engineering: A*, vol. 758, pp. 60–70, 2019.
[6] P. K. Romano, N. E. Horelik, B. R. Herman, A. G. Nelson, B. Forget, and K. Smith, "Openmc: A state-of-the-art monte carlo code for research and development", *Annals of Nuclear Energy*, vol. 82, pp. 90–97, 2015.
[7] H. Vega-Carrillo, V. Hernández-Dávila, T. Rivera, and A. Sánchez, "Nuclear and dosimetric features of an isotopic neutron source", *Radiation Physics and Chemistry*, vol. 95, pp. 122–124, 2014.
[8] Y.-Q. Shi, Q.-F. Zhu, and H. Tao, "Review and research of the neutron source multiplication method in nuclear critical safety", *Nuclear technology*, vol. 149, no. 1, pp. 122–127, 2005.